AIMS Mathematics, 10(10): 23235–23260.
DOI: 10.3934/math.20251031
Received: 17 June 2025
Revised: 18 September 2025
Accepted: 24 September 2025
Published: 14 October 2025

https://www.aimspress.com/journal/Math

Research article

Modeling adenovirus transmission dynamics using a SEVAIR framework with asymptomatic and vaccinated classes

Mohamed S. Algolam[1], Ashraf A. Qurtam[2], Arshad Ali[3], Khaled Aldwoah[4,*], Amer Alsulami[5], Mohammed Rabih[6,*] and Mahmoud M. Abdelwahab[7]

[1] Department of Mathematics, College of Science, University of Ha'il, Ha'il 55473, Saudi Arabia
[2] Biology Department, College of Science, Imam Mohammad Ibn Saud Islamic University (IMSIU), Riyadh, 11623, Saudi Arabia
[3] Department of Mathematics, University of Malakand, Chakdara Dir(L), Khyber Pakhtunkhwa 18800, Pakistan
[4] Department of Mathematics, Faculty of Science, Islamic University of Madinah, Madinah 42351, Saudi Arabia
[5] Department of Mathematics, Turabah University College, Taif University, Taif, Saudi Arabia
[6] Department of Mathematics, College of Science, Qassim University, Buraydah 51452, Saudi Arabia
[7] Department of Mathematics and Statistics, Imam Mohammad Ibn Saud Islamic University (IMSIU), Riyadh 11623, Saudi Arabia

* **Correspondence:** Email: aldwoah@iu.edu.sa, m.fadlallah@qu.edu.sa.

Abstract: In this work, we extended the classical Susceptible–Exposed–Vaccinated–Infected–Recovered (SEVIR) framework by incorporating an asymptomatic class, leading to the formulation of a new Susceptible–Exposed–Vaccinated–Asymptomatic–Infected–Recovered (SEVAIR) model that more accurately reflects the transmission characteristics of adenovirus. To account for memory effects and capture complex temporal behavior, the model was developed using the fractal-fractional Caputo-Fabrizio derivative with a power-law kernel. Existence and stability of solutions based on fixed point theory and Hyers-Ulam stability criteria were derived. Both the disease-free and endemic equilibrium states were derived, and their local stability properties were examined. Additionally, the basic reproduction number was computed to understand the disease's spread threshold. The theoretical results were supported by numerical simulations, which were performed using a modified Adams-Bashforth approach tailored for the fractional framework.

Keywords: SEVAIR epidemic model; adenovirus dynamics; asymptomatic transmission; disease-free and endemic equilibrium analysis; solution stability; Adams-Bashforth scheme; simulations
Mathematics Subject Classification: 26A33, 34A08, 34A12

1. Introduction

Adenoviruses, members of the Adenoviridae family, are common viral pathogens capable of causing diverse illnesses, including respiratory, gastrointestinal, and ocular infections. Among these, adenoviral conjunctivitis represents one of the most frequent clinical manifestations. It occurs due to inflammation of the conjunctiva, the transparent membrane covering the sclera and lining the eyelids, which can result from viral, bacterial, or allergenic exposure. Conjunctivitis presents in multiple forms, with allergic conjunctivitis being particularly associated with environmental irritants such as pollen, dust mites, animal dander, contact lenses, or chemicals [1, 2].

Transmission typically occurs through direct or indirect contact with infected individuals, contaminated objects, or exposure to ocular and respiratory secretions. Maternal infections such as chlamydia and gonorrhea may also contribute to neonatal cases. A severe form, acute hemorrhagic conjunctivitis (AHC), is characterized by abrupt symptom onset within one to three days, with clinical features including tearing, eye discomfort, photophobia, sore throat, eyelid swelling, and sometimes purulent discharge [3]. Management strategies mainly emphasize symptom control and containment of transmission through hygienic practices, temporary isolation, and, in some cases, antibiotic eye drops. AHC tends to spread rapidly in tropical climates, particularly during rainy seasons where humidity favors viral persistence [4–6]. Countries such as Thailand frequently report seasonal outbreaks [7, 8]. Public health guidelines underscore the importance of isolation measures, including medical leave and school absenteeism during the infectious phase, to reduce secondary transmission [9–12].

Mathematical modeling provides a powerful framework for analyzing the dynamics of infectious diseases and guiding intervention strategies. Traditionally, epidemiological systems have been described using classical integer-order differential equations. However, these models often fall short in capturing memory, heterogeneity, and long-term persistence inherent in biological processes [13–17]. The emergence of fractional calculus has significantly advanced the modeling of such complex dynamics, enabling the inclusion of non-local effects and hereditary properties. Recent works have emphasized the importance of fractional-order epidemic models in providing richer insights into disease spread, particularly by accounting for memory and anomalous transmission patterns [18–22].

Moreover, fractional models have been adapted to multi-strain diseases and non-biological epidemics. For example, Yaagoub proposed a fractional two-strain Susceptible–Vaccinated–Latent–Infected–Recovered (SVLIR) framework with vaccination and quarantine interventions [23], while related research applied fractional calculus to the study of computer virus propagation [24]. These examples illustrate the versatility and applicability of fractional operators in diverse domains. Within this context, Caputo and Fabrizio introduced a non-singular fractional derivative that avoids the limitations of singular kernels [25]. More recent developments have integrated fractal structures with fractional operators [26], further enriching the study of diverse epidemiological systems [27, 28].

Several Susceptible–Exposed–Infected–Recovered (SEIR)-type models have been proposed for conjunctivitis transmission. For instance, [6] formulated a classical SEIR model, later extended by [29] into a SEVIR framework that incorporated vaccination and the Atangana-Baleanu derivative. Additional variations explored treatment strategies [30] and waning immunity with reinfection [31]. While insightful, these models generally overlook the role of asymptomatic carriers, who may silently sustain transmission chains in closed populations such as schools, hospitals, and military camps.

To address this gap, we extend the SEVIR model by introducing an asymptomatic class, resulting

in the SEVAIR framework. The new compartment accounts for infected individuals who show no clinical symptoms but remain infectious. This modification enables a more realistic assessment of adenovirus dynamics, particularly the hidden contribution of asymptomatic spread. Additionally, the model is formulated using the fractal-fractional Caputo-Fabrizio derivative with power-law kernel enabling us to capture both non-local memory effects and fractal-like heterogeneity observed in real-world epidemic processes. Adenovirus transmission often exhibits delays, long-term dependencies, and non-exponential decay of infection rates, which cannot be fully captured by classical integer-order or standard fractional models. The fractal-fractional operator provides a flexible framework to account for these complex features.

The main contributions of this study can be summarized as follows:

- We develop a novel SEVAIR model that extends the fractional-order SEVIR framework [29], by explicitly incorporating asymptomatic individuals.
- We employ the fractal-fractional Caputo-Fabrizio operator with a power-law kernel to capture non-local memory and heterogeneous disease dynamics.
- We analyze equilibrium states, calculate the basic reproduction number, and analyze the stability of the equilibrium points.
- We investigate the existence and stability of the model using fixed-point theory and Hyers-Ulam (H-U) stability concepts.
- We develop a numerical scheme for the solution of the proposed model.
- We support theoretical analysis with numerical simulations that illustrate both fractional and fractal-fractional dynamics.
- We provide schematic flow diagrams and simulation results to highlight the interplay between symptomatic and asymptomatic pathways.

The structure of the paper is outlined as follows. In Section 2, the proposed model is presented. Section 3 presents the required preliminaries and supporting mathematical concepts. In Section 4, we carry out the theoretical analysis, focusing on equilibrium states, the basic reproduction number, and stability properties. The existence and uniqueness of solutions are discussed in Section 5. Section 6 presents H-U stability criteria of the proposed SEVAIR model. Section 7 is devoted to the numerical scheme for the solution of the SEVAIR model. Section 8 presents a simulation and analysis. Lastly, Section 9 summarizes the main results and outlines potential avenues for future research.

2. Model formulation

In this section, we formulate the proposed model as follows:

$$\begin{cases} {}^{FFCF}D_{\theta}^{\sigma,\varrho}S(\theta) = N\rho - \zeta IS(\theta) - \zeta_a AS(\theta) - \beta S(\theta), \\ {}^{FFCF}D_{\theta}^{\sigma,\varrho}E(\theta) = \zeta IS(\theta) + \zeta_a AS(\theta) - \eta E(\theta) - \beta E(\theta), \\ {}^{FFCF}D_{\theta}^{\sigma,\varrho}V(\theta) = \eta E(\theta) - \gamma V(\theta) - \beta V(\theta), \\ {}^{FFCF}D_{\theta}^{\sigma,\varrho}A(\theta) = k\gamma V(\theta) - (\tau + \beta)A(\theta), \\ {}^{FFCF}D_{\theta}^{\sigma,\varrho}I(\theta) = (1-k)\gamma V(\theta) + \tau A - (b + q + \beta)I(\theta), \\ {}^{FFCF}D_{\theta}^{\sigma,\varrho}R(\theta) = (b+q)I(\theta) - \beta R(\theta), \\ S(0) = S_0,\ E(0) = E_0,\ V(0) = V_0,\ A(0) = A_0,\ I(0) = I_0,\ R(0) = R_0, \end{cases} \tag{2.1}$$

where the notion ${}^{FFCF}D_{\theta}^{\sigma,\varrho}$ denotes the Caputo-Fabrizio fractal-fractional differential operator, $S(\theta)$ corresponds to individuals who are susceptible, $E(\theta)$ represents those who have been exposed, $V(\theta)$ corresponds to vaccinated individuals, $I(\theta)$ corresponds to individuals infected with conjunctivitis, $A(\theta)$ is the class of asymptomatic individuals, and $R(\theta)$ indicates those who have recovered at time θ.

In Figure 1, a flowchart depicting the movement of individuals among the SEVAIR compartments is included to visually represent the structure and propagation pathway of the proposed model.

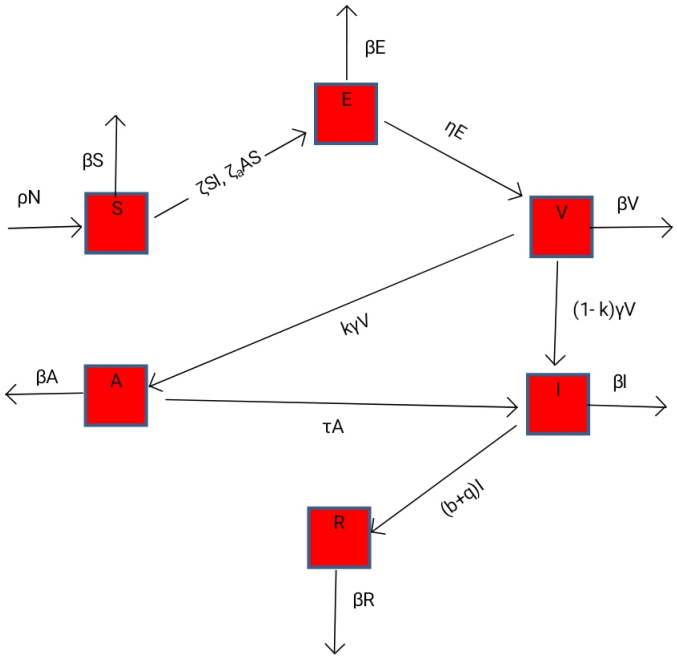

Figure 1. Flowchart of the proposed model (2.1).

Many of the parameter values employed in the fractal-fractional SEVAIR model are retained from the fractional-order SEVIR model [29]. This approach ensures consistency with earlier studies and facilitates a direct comparison of the dynamical behaviors under different derivative operators. Furthermore, the extension of the model to incorporate the asymptomatic class within the fractal-fractional framework highlights the novelty of our work, while maintaining biological interpretability of the parameters. A more detailed parameter identification framework, such as that presented in [32], could be considered in future work for refined data-driven analysis.

3. Basic results

In this section, we present the essential theoretical background and analytical tools relevant to our study. These include definitions from fractal-fractional calculus, specifically involving the fractal-fractional Caputo–Fabrizio (FFCF) derivative and the fractal-fractional Riemann–Liouville (FFRL) integral, each defined with distinct kernel functions.

Definition 3.1. [26] Let $\vartheta(\theta)$ be a continuous function that is fractally differentiable on the interval

(a, b) of order ϱ. Then, its FFCF derivative of order σ is defined using a power-law kernel:

$$^{FFCF}D^{\sigma,\varrho}\vartheta(\theta) = \frac{1}{\Gamma(1-\sigma)}\int_0^\theta \frac{d}{dy^\varrho}\vartheta(y)(\theta-y)^{-\sigma}dy, \quad \theta \in [0,T], \tag{3.1}$$

where $0 < \sigma, \varrho \leq 1$, and

$$\frac{d}{dy^\varrho}\vartheta(y) = \lim_{\theta\to y}\frac{\vartheta(\theta)-\vartheta(y)}{\theta^\varrho - y^\varrho}. \tag{3.2}$$

Definition 3.2. [26] Let $\vartheta \in C(0,T)$ and then the FFRL integral of the function $\vartheta(\theta)$ with a power-law kernel is given as

$$^{FFRL}I^{\sigma,\varrho}\vartheta(\theta) = \frac{\varrho}{\Gamma(\sigma)}\int_a^\theta (\theta-y)^{\sigma-1}y^{\varrho-1}\vartheta(y)dy. \tag{3.3}$$

Theorem 3.3. *Let $\mathbb{Q}_1$ and $\mathbb{Q}_2$ be two operators where $\mathbb{Q}_1$ is a contraction and $\mathbb{Q}_2$ is completely continuous over a closed and bounded subset of a Banach space. Then, the operator equation $\mathbb{Q}_1\mathcal{F} + \mathbb{Q}_2\mathcal{F} = \mathcal{F}$ admits at least one solution.*

Definition 3.4. The Adams-Bashforth method for solving ordinary differential equations numerically can be described by the following scheme:

$$x_{p+1} = x_p + h\sum_{i=1}^{r} a_i f(t_p + ih, x_p + ih),$$

where x_p represents the numerical approximation at time t_p, h denotes the time step size, $f(x,\vartheta)$ is the given ordinary differential equation, and a_i are method-specific coefficients that depend on the order of the method.

In the next section, we obtain equilibrium points and compute the basic reproduction number.

4. Equilibria, basic reproduction number, and local stability analysis

In this section, we analyze disease-free equilibrium (DFE), endemic equilibrium (EE) points, and their stability. Moreover, we compute the basic reproduction number $\mathcal{R}_0$ that provides a threshold condition for disease spread. The positivity of the model is also presented in this section.

It is important to note that the determination of equilibrium points is independent of the fractional or fractal-fractional order of the derivative. The equilibria are obtained by solving algebraic equations derived from the system, which remain identical to those of the corresponding integer-order model.

4.1. Equilibria and basic reproduction number

To determine the equilibrium points, we set all the right-hand sides of the differential equations in the system to zero.

$$\begin{cases} N\rho - \zeta IS - \zeta_a AS - \beta S = 0, \\ \zeta IS + \zeta_a AS - \eta E - \beta E = 0, \\ \eta E - \gamma V - \beta V = 0, \\ k\gamma V - (\tau+\beta)A = 0, \\ (1-k)\gamma V + \tau A - (b+q+\beta)I = 0, \\ (b+q)I - \beta R = 0. \end{cases} \tag{4.1}$$

Disease-free equilibrium (DFE):

At the DFE, there is no infection in the population, and hence we get

$$S^0 = \frac{N\rho}{\beta}. \tag{4.2}$$

Thus, we have the following DFE:

$$(S^0, E^0, V^0, A^0, I^0, R^0) = \left(\frac{N\rho}{\beta},\ 0,\ 0,\ 0,\ 0,\ 0\right).$$

Before proceeding to the derived condition for existence of endemic equilibrium, we find the basic reproduction number.

Basic reproduction number:

We derive the basic reproduction number $\mathcal{R}_0$ using the next-generation matrix method for the SEVAIR model, which is governed by the following system:

$$\begin{cases} {}^{FFCF}D_\theta^{\sigma,\varrho}S(\theta) = N\rho - \zeta IS(\theta) - \zeta_a AS(\theta) - \beta S(\theta), \\ {}^{FFCF}D_\theta^{\sigma,\varrho}E(\theta) = \zeta IS(\theta) + \zeta_a AS(\theta) - \eta E(\theta) - \beta E(\theta), \\ {}^{FFCF}D_\theta^{\sigma,\varrho}V(\theta) = \eta E(\theta) - \gamma V(\theta) - \beta V(\theta), \\ {}^{FFCF}D_\theta^{\sigma,\varrho}A(\theta) = k\gamma V(\theta) - (\tau + \beta)A(\theta), \\ {}^{FFCF}D_\theta^{\sigma,\varrho}I(\theta) = (1-k)\gamma V(\theta) + \tau A(\theta) - (p + q + \beta)I(\theta), \\ {}^{FFCF}D_\theta^{\sigma,\varrho}R(\theta) = (p+q)I(\theta) - \beta R(\theta). \end{cases} \tag{4.3}$$

We identify the infected compartments contributing to new infections as:

$$\mathbf{x} = \begin{bmatrix} E \\ V \\ A \\ I \end{bmatrix}.$$

At the DFE, all infected compartments are zero:

$$E = V = A = I = 0, \quad S = S^* = \frac{N\rho}{\beta}, \quad R = 0.$$

Now, we derive the new infection matrix $\mathcal{F}(x)$. Only the exposed class receives new infections and hence

$$\mathcal{F} = \begin{bmatrix} \zeta IS^* + \zeta_a AS^* \\ 0 \\ 0 \\ 0 \end{bmatrix}.$$

The transition matrix $\mathcal{V}(x)$ is obtained as:

$$\mathcal{V} = \begin{bmatrix} (\eta + \beta)E \\ -\eta E + (\gamma + \beta)V \\ -k\gamma V + (\tau + \beta)A \\ -(1-k)\gamma V - \tau A + (p + q + \beta)I \end{bmatrix}.$$

The Jacobian of $\mathcal{F}$ at the DFE is given as:

$$J_{\mathcal{F}} = \frac{\partial \mathcal{F}}{\partial(E, V, A, I)} = \begin{bmatrix} 0 & 0 & \zeta_a S^* & \zeta S^* \\ 0 & 0 & 0 & 0 \\ 0 & 0 & 0 & 0 \\ 0 & 0 & 0 & 0 \end{bmatrix}.$$

The Jacobian of $\mathcal{V}$ at the DFE is given as:

$$J_{\mathcal{V}} = \begin{bmatrix} \eta + \beta & 0 & 0 & 0 \\ -\eta & \gamma + \beta & 0 & 0 \\ 0 & -k\gamma & \tau + \beta & 0 \\ 0 & -(1-k)\gamma & -\tau & p + q + \beta \end{bmatrix}.$$

By computing $J_{\mathcal{F}} J_{\mathcal{V}}^{-1}$ explicitly, we obtain the following basic reproduction number ($\mathcal{R}_0$):

$$\mathcal{R}_0 = \frac{S^* \eta \gamma}{(\eta + \beta)(\gamma + \beta)} \left(\zeta_a \cdot \frac{k}{\tau + \beta} + \zeta \left(\frac{(1-k)}{p + q + \beta} + \frac{k\tau}{(\tau + \beta)(p + q + \beta)} \right) \right).$$

Substituting $S^* = \dfrac{N\rho}{\beta}$, we obtain:

$$\mathcal{R}_0 = \frac{N\rho\eta\gamma}{\beta(\eta + \beta)(\gamma + \beta)} \left[\zeta_a \cdot \frac{k}{\tau + \beta} + \zeta \left(\frac{(1-k)}{p + q + \beta} + \frac{k\tau}{(\tau + \beta)(p + q + \beta)} \right) \right].$$

This is the expression for $\mathcal{R}_0$, which determines whether the infection will spread in the population. If $\mathcal{R}_0 > 1$, an epidemic occurs; otherwise, the disease will die out.

Necessary condition for the existence of an endemic equilibrium (EE):

Setting the right-hand sides of system (4.3) to zero gives the steady-state algebraic system

$$\begin{cases} N\rho - \zeta I^* S^* - \zeta_a A^* S^* - \beta S^* = 0, \\ \zeta I^* S^* + \zeta_a A^* S^* - (\eta + \beta) E^* = 0, \\ \eta E^* - (\gamma + \beta) V^* = 0, \\ k\gamma V^* - (\tau + \beta) A^* = 0, \\ (1-k)\gamma V^* + \tau A^* - (p + q + \beta) I^* = 0, \\ (p + q) I^* - \beta R^* = 0. \end{cases} \tag{4.4}$$

From the third, fourth, and fifth equations of (4.4), we obtain direct linear relations expressing V^*, A^*, I^* in terms of E^*:

$$V^* = \frac{\eta}{\gamma + \beta} E^*, \qquad A^* = \frac{k\gamma}{\tau + \beta} V^* = \frac{k\gamma\eta}{(\gamma + \beta)(\tau + \beta)} E^*,$$

and

$$I^* = \frac{(1-k)\gamma V^* + \tau A^*}{p + q + \beta} = \frac{(1-k)\gamma\eta + \tau \cdot (k\gamma\eta/(\tau + \beta))/(\gamma + \beta)}{p + q + \beta} E^*.$$

Collecting terms, the explicit expression for I^* in terms of E^* is

$$I^* = \frac{\gamma\eta}{(\gamma + \beta)(p + q + \beta)} \left[(1-k) + \frac{k\tau}{\tau + \beta} \right] E^* = \frac{\gamma\eta}{(\gamma + \beta)(p + q + \beta)} \cdot \frac{(1-k)(\tau + \beta) + k\tau}{\tau + \beta} E^*.$$

Substitute A^* and I^* into the second equation of (4.4). For an endemic equilibrium with $E^* > 0$ we obtain the relation

$$(\eta+\beta) = S^*\left(\zeta I^*/E^* + \zeta_a A^*/E^*\right) = S^*\left[\zeta \cdot \frac{\gamma\eta}{(\gamma+\beta)(p+q+\beta)} \cdot \frac{(1-k)(\tau+\beta)+k\tau}{\tau+\beta} + \zeta_a \cdot \frac{k\gamma\eta}{(\gamma+\beta)(\tau+\beta)}\right].$$

Rearranging yields an explicit expression for the susceptible population at the EE:

$$S^* = \frac{\eta+\beta}{\zeta\dfrac{\gamma\eta}{(\gamma+\beta)(p+q+\beta)} \cdot \dfrac{(1-k)(\tau+\beta)+k\tau}{\tau+\beta} + \zeta_a\dfrac{k\gamma\eta}{(\gamma+\beta)(\tau+\beta)}} = \frac{\eta+\beta}{C}, \tag{4.5}$$

where

$$C = \zeta\frac{\gamma\eta}{(\gamma+\beta)(p+q+\beta)}\frac{(1-k)(\tau+\beta)+k\tau}{\tau+\beta} + \zeta_a\frac{k\gamma\eta}{(\gamma+\beta)(\tau+\beta)}. \tag{4.6}$$

From the first equation of (4.4), we also have

$$S^* = \frac{N\rho}{\beta+\zeta I^*+\zeta_a A^*}. \tag{4.7}$$

Using the previously derived relations

$$I^* = \frac{\gamma\eta}{(\gamma+\beta)(p+q+\beta)}\frac{(1-k)(\tau+\beta)+k\tau}{\tau+\beta}E^*, \qquad A^* = \frac{k\gamma\eta}{(\gamma+\beta)(\tau+\beta)}E^*, \tag{4.8}$$

we compute

$$\begin{aligned}\zeta I^* + \zeta_a A^* &= \left(\zeta\frac{\gamma\eta}{(\gamma+\beta)(p+q+\beta)}\frac{(1-k)(\tau+\beta)+k\tau}{\tau+\beta} + \zeta_a\frac{k\gamma\eta}{(\gamma+\beta)(\tau+\beta)}\right)E^* \\ &= CE^*.\end{aligned} \tag{4.9}$$

Hence (4.7) becomes

$$S^* = \frac{N\rho}{\beta+CE^*}. \tag{4.10}$$

From the second steady–state equation, we already obtained

$$S^* = \frac{\eta+\beta}{C}. \tag{4.11}$$

Equating (4.10) and (4.11) gives

$$\frac{N\rho}{\beta+CE^*} = \frac{\eta+\beta}{C}. \tag{4.12}$$

Cross-multiplying,

$$CN\rho = (\eta+\beta)(\beta+CE^*). \tag{4.13}$$

Expanding the right-hand side,

$$CN\rho = (\eta+\beta)\beta + (\eta+\beta)CE^*. \tag{4.14}$$

Subtracting $(\eta+\beta)\beta$ from both sides,

$$CN\rho - (\eta+\beta)\beta = (\eta+\beta)CE^*. \tag{4.15}$$

Dividing by $C(\eta+\beta)$ yields

$$E^* = \frac{CN\rho - \beta(\eta+\beta)}{C(\eta+\beta)}. \tag{4.16}$$

For an endemic equilibrium (EE), we require $E^* > 0$, which is equivalent to

$$CN\rho - \beta(\eta+\beta) > 0 \quad \Longleftrightarrow \quad N\rho C > \beta(\eta+\beta). \tag{4.17}$$

Substituting the definition (4.6) of C gives

$$N\rho\left(\zeta\frac{\gamma\eta}{(\gamma+\beta)(p+q+\beta)}\frac{(1-k)(\tau+\beta)+k\tau}{\tau+\beta} + \zeta_a\frac{k\gamma\eta}{(\gamma+\beta)(\tau+\beta)}\right) > \beta(\eta+\beta). \tag{4.18}$$

Simplifying the last inequality and re-arranging the terms, we obtain

$$\frac{N\rho\eta\gamma}{(\gamma+\beta)}\left[\zeta_a\cdot\frac{k}{\tau+\beta} + \zeta\left(\frac{(1-k)}{p+q+\beta} + \frac{k\tau}{(\tau+\beta)(p+q+\beta)}\right)\right] > \beta(\eta+\beta).$$

Dividing both sides by $\beta(\eta+\beta)$ yields the equivalent condition $\mathcal{R}_0 > 1$, where $\mathcal{R}_0$ is the reproduction number. Thus we obtain the standard existence result:

Proposition 1. *The model admits the DFE $\mathcal{E}_0 = (S^*, 0, 0, 0, 0, 0)$ with $S^* = N\rho/\beta$. A positive EE $\mathcal{E}^*$ (with $E^* > 0$) exists if and only if $\mathcal{R}_0 > 1$.*

The numerical EE point for the given set of parameter values is given by

$$(S^*, E^*, V^*, A^*, I^*, R^*) \approx (28.8948,\ 0.13642,\ 1.0221,\ 0.81595,\ 0.12013,\ 969.0106).$$

4.2. Local stability analysis

To analyze the local stability of the equilibrium points, we compute the Jacobian matrix of the system. Let $f_1, f_2, \ldots, f_6$ denote the right-hand sides of the model equations for (S, E, V, A, I, R). The Jacobian is

$$J = \begin{bmatrix} \frac{\partial f_1}{\partial S} & \frac{\partial f_1}{\partial E} & \frac{\partial f_1}{\partial V} & \frac{\partial f_1}{\partial A} & \frac{\partial f_1}{\partial I} & \frac{\partial f_1}{\partial R} \\ \frac{\partial f_2}{\partial S} & \frac{\partial f_2}{\partial E} & \frac{\partial f_2}{\partial V} & \frac{\partial f_2}{\partial A} & \frac{\partial f_2}{\partial I} & \frac{\partial f_2}{\partial R} \\ \frac{\partial f_3}{\partial S} & \frac{\partial f_3}{\partial E} & \frac{\partial f_3}{\partial V} & \frac{\partial f_3}{\partial A} & \frac{\partial f_3}{\partial I} & \frac{\partial f_3}{\partial R} \\ \frac{\partial f_4}{\partial S} & \frac{\partial f_4}{\partial E} & \frac{\partial f_4}{\partial V} & \frac{\partial f_4}{\partial A} & \frac{\partial f_4}{\partial I} & \frac{\partial f_4}{\partial R} \\ \frac{\partial f_5}{\partial S} & \frac{\partial f_5}{\partial E} & \frac{\partial f_5}{\partial V} & \frac{\partial f_5}{\partial A} & \frac{\partial f_5}{\partial I} & \frac{\partial f_5}{\partial R} \\ \frac{\partial f_6}{\partial S} & \frac{\partial f_6}{\partial E} & \frac{\partial f_6}{\partial V} & \frac{\partial f_6}{\partial A} & \frac{\partial f_6}{\partial I} & \frac{\partial f_6}{\partial R} \end{bmatrix}. \tag{4.19}$$

Substituting the partial derivatives gives

$$J = \begin{bmatrix} -\beta - A\zeta_a - I\zeta & 0 & 0 & -S\zeta_a & -S\zeta & 0 \\ A\zeta_a + I\zeta & -\beta-\eta & 0 & S\zeta_a & S\zeta & 0 \\ 0 & \eta & -\gamma-\beta & 0 & 0 & 0 \\ 0 & 0 & \gamma k & -\beta-\tau & 0 & 0 \\ 0 & 0 & -\gamma(1-k) & \tau & -\beta-b-q & 0 \\ 0 & 0 & 0 & 0 & b+q & -\beta \end{bmatrix}. \tag{4.20}$$

At the disease-free equilibrium (DFE) $\mathcal{E}_0 = (S, E, V, A, I, R) = (N, 0, 0, 0, 0, 0)$, we substitute $S = N$, $A = 0$, and $I = 0$, yielding

$$J_0 = \begin{bmatrix} -\beta & 0 & 0 & -N\zeta_a & -N\zeta & 0 \\ 0 & -\beta-\eta & 0 & N\zeta_a & N\zeta & 0 \\ 0 & \eta & -\gamma-\beta & 0 & 0 & 0 \\ 0 & 0 & \gamma k & -\beta-\tau & 0 & 0 \\ 0 & 0 & -\gamma(1-k) & \tau & -\beta-b-q & 0 \\ 0 & 0 & 0 & 0 & b+q & -\beta \end{bmatrix}. \tag{4.21}$$

The characteristic equation is obtained by subtracting ΥI from J_0 (where Υ denotes the eigenvalue parameter and I is the 6×6 identity matrix) and computing the determinant:

$$|J_0 - \Upsilon I| = \begin{vmatrix} -\Upsilon-\beta & 0 & 0 & -\zeta_a N & -\zeta N & 0 \\ 0 & -\Upsilon-\beta-\eta & 0 & \zeta_a N & \zeta N & 0 \\ 0 & \eta & -\Upsilon-\gamma-\beta & 0 & 0 & 0 \\ 0 & 0 & \gamma k & -\Upsilon-\beta-\tau & 0 & 0 \\ 0 & 0 & \gamma(k-1) & \tau & -\Upsilon-\beta-p-q & 0 \\ 0 & 0 & 0 & 0 & p+q & -\Upsilon-\beta \end{vmatrix}. \tag{4.22}$$

Solving $|J_0 - \Upsilon I| = 0$ gives the eigenvalues of the DFE. Using the parameter values from Table 1, we find:

$$\Upsilon_1 = -0.00004215, \quad \Upsilon_2 = -0.00004215, \quad \Upsilon_3 = 0.0305495, \quad \Upsilon_4 = -0.0774637 + 0.261544\,i,$$

$$\Upsilon_5 = -0.0774637 - 0.261544\,i, \quad \Upsilon_6 = -0.575791.$$

Table 1. Parameters and their descriptions.

Parameters	Definition	Parameters values	Source
N	Total population	1000	Assumed
ζ	Transmission rate for AHC	0.005	Assumed
ζ_a	Transmission rate by asymptomatic	0.001	Assumed
k	Vaccinated-exposed to asymptomatic proportion	0.4	[29]
τ	Asymptomatic-to-symptomatic rate	0.02	Assumed
ρ	Birth rate	0.00004215	[29]
β	Natural death rate	0.00004215	[29]
η	Incubation rate for AHC	0.3	[29]
γ	Vaccinated-to-infected incidence rate	0.04	[29]
b	Recovery rate for symptomatic individuals	0.04	[29]
q	Quarantine rate for symptomatic individuals	0.3	[29]

Since $\Upsilon_3 > 0$, the disease-free equilibrium is unstable, implying that the infection can invade the population when introduced. For the endemic equilibrium $\mathcal{E}^* = (S^*, E^*, V^*, A^*, I^*, R^*)$, we evaluate (4.20) at the starred values. Substituting these and the parameter values yields:

$$\Upsilon_1 = -0.00004215, \quad \Upsilon_2 = -0.000606315 + 0.00455853\,i, \quad \Upsilon_3 = -0.000606315 - 0.00455853\,i,$$

$$\Upsilon_4 = -0.050494, \quad \Upsilon_5 = -0.32496 + 0.0549824\,i, \quad \Upsilon_6 = -0.32496 - 0.0549824\,i.$$

All eigenvalues have negative real parts, confirming that $\mathcal{E}^*$ is locally asymptotically stable. Small perturbations decay over time, and the trajectories return to $\mathcal{E}^*$, with complex conjugate pairs indicating damped oscillations in the transient dynamics.

Positivity of the model:

We describe the positivity of the model as:

$$\begin{cases} {}^{FFCF}D_{\theta}^{\sigma,\varrho}S(\theta) = N\rho \geq 0, \\ {}^{FFCF}D_{\theta}^{\sigma,\varrho}E(\theta) = \zeta IS + \zeta_a AS \geq 0, \\ {}^{FFCF}D_{\theta}^{\sigma,\varrho}V(\theta) = \eta E \geq 0, \\ {}^{FFCF}D_{\theta}^{\sigma,\varrho}A(\theta) = k\gamma V \geq 0, \\ {}^{FFCF}D_{\theta}^{\sigma,\varrho}I(\theta) = \gamma V + \tau A, \\ {}^{FFCF}D_{\theta}^{\sigma,\varrho}R(\theta) = (b+q)I \geq 0. \end{cases} \tag{4.23}$$

Theorem 4.1. *Every solution of* (4.23) *is bounded and it exists inside the boundary region as given by*

$$\Lambda = \left\{ (S, E, V, A, I, R) \in \mathbb{R}_+^6 : N = S + E + V + A + I + R \leq \frac{N\rho}{d_r} \right\}.$$

Proof. We have

$$N = S + E + V + A + I + R. \tag{4.24}$$

Applying the differential operator ${}^{FFCF}D_{\theta}^{\sigma,\varrho}$ to both sides, we have

$${}^{FFCF}D_{\theta}^{\sigma,\varrho}N = {}^{FFCF}D_{\theta}^{\sigma,\varrho}S + {}^{FFCF}D_{\theta}^{\sigma,\varrho}E + {}^{FFCF}D_{\theta}^{\sigma,\varrho}V + {}^{FFCF}D_{\theta}^{\sigma,\varrho}A + {}^{FFCF}D_{\theta}^{\sigma,\varrho}I + {}^{FFCF}D_{\theta}^{\sigma,\varrho}R. \tag{4.25}$$

Using the corresponding values, we have

$${}^{FFCF}D_{\theta}^{\sigma,\varrho}N = N\rho - N\beta. \tag{4.26}$$

Taking the limit $n \to 0$, and applying the Laplace transform, we have

$$N \leq \frac{N\rho}{\beta}. \tag{4.27}$$

□

In the next section, we investigate the existence and uniqueness of solutions.

5. Fixed-point results

We proceed with fixed point theory and functional analysis to examine the existence and uniqueness of solutions for the proposed model (2.1).

Let the interval $[0, T]$ be represented by $\mathbb{I}$ and we define a suitable Banach space accordingly as below:

$$\mathfrak{B} = C(\mathbb{I}, \mathbb{R}^+) \times C(\mathbb{I}, \mathbb{R}^+) \times C(\mathbb{I}, \mathbb{R}^+) \times C(\mathbb{I}, \mathbb{R}^+) \times C(\mathbb{I}, \mathbb{R}^+) \times C(\mathbb{I}, \mathbb{R}^+)$$

equipped with the following norm:

$$\|\vartheta\| = \max\left\{|S(\theta)| + |E(\theta)| + |V(\theta)| + |A(\theta)| + |I(\theta)| + |R(\theta)|\right\};$$

$S, E, V, A, I, R \in \mathfrak{B}$.

Problem (2.1) can be formulated as

$$\begin{cases} {}^{FFCF}D_{\theta}^{\sigma,\varrho}\vartheta(\theta) = \vartheta_1(\theta, S, E, V, A, I, R), \\ {}^{FFCF}D_{\theta}^{\sigma,\varrho}\vartheta(\theta) = \vartheta_2(\theta, S, E, V, A, I, R), \\ {}^{FFCF}D_{\theta}^{\sigma,\varrho}\vartheta(\theta) = \vartheta_3(\theta, S, E, V, A, I, R), \\ {}^{FFCF}D_{\theta}^{\sigma,\varrho}\vartheta(\theta) = \vartheta_4(\theta, S, E, V, A, I, R), \\ {}^{FFCF}D_{\theta}^{\sigma,\varrho}\vartheta(\theta) = \vartheta_5(\theta, S, E, V, A, I, R), \\ {}^{FFCF}D_{\theta}^{\sigma,\varrho}\vartheta(\theta) = \vartheta_6(\theta, S, E, V, A, I, R). \end{cases} \tag{5.1}$$

System (5.1) can be given in a compact form as

$${}^{FFCF}D_{\theta}^{\sigma,\varrho}\vartheta(\theta) = \begin{cases} g(\theta, \vartheta(\theta)), \\ \vartheta(0) = \vartheta_0, \quad \theta \in \mathbb{I}, \end{cases} \tag{5.2}$$

where the vector $\vartheta(\theta) = (S, E, V, A, I, R)$ denotes the variable with specified initial condition ϑ_0 and the variable function g takes the form:

$$g(\theta, \vartheta(\theta)) = \begin{bmatrix} \vartheta_1(\theta, S, E, V, A, I, R) \\ \vartheta_2(\theta, S, E, V, A, I, R) \\ \vartheta_3(\theta, S, E, V, A, I, R) \\ \vartheta_4(\theta, S, E, V, A, I, R) \\ \vartheta_5(\theta, S, E, V, A, I, R) \\ \vartheta_6(\theta, S, E, V, A, I, R) \end{bmatrix}, \ \vartheta(\theta) = \begin{bmatrix} \vartheta_1 \\ \vartheta_2 \\ \vartheta_3 \\ \vartheta_4 \\ \vartheta_5 \\ \vartheta_6 \end{bmatrix} = \begin{bmatrix} N\rho - \zeta IS(\theta) - \zeta_a AS(\theta) - \beta S(\theta), \\ \zeta IS(\theta) + \zeta_a AS(\theta) - \eta E(\theta) - \beta E(\theta), \\ \eta E(\theta) - \gamma V(\theta) - \beta V(\theta), \\ k\gamma V(\theta) - (\tau + \beta)A(\theta), \\ (1-k)\gamma V(\theta) + \tau A - (b + q + \beta)I(\theta), \\ (b + q)I(\theta) - \beta R(\theta), \end{bmatrix},$$

and

$$\vartheta_0 = \begin{bmatrix} S_0 \\ E_0 \\ V_0 \\ A_0 \\ I_0 \\ R_0 \end{bmatrix}.$$

Lemma 5.1. *Problem*

$${}^{FFCF}D_{\theta}^{\sigma,\varrho}\vartheta(\theta) = \begin{cases} \varphi(\theta), & 0 < \sigma, \varrho \leq 1, \ \text{if } \theta \in [0, T], \\ & \vartheta(0) = \vartheta_0, \end{cases} \tag{5.3}$$

has the solution

$$\vartheta(\theta) = \vartheta_0 + \frac{\varrho(1-\sigma)\theta^{\varrho-1}\varphi(\theta)}{M(\sigma)} + \frac{\sigma\varrho}{M(\sigma)}\int_0^{\theta} y^{\sigma-1}\varphi(y)dy, \quad \theta \in \mathbb{I}. \tag{5.4}$$

Corollary 1. *By Lemma 5.1, the solution to the problem* (5.2) *of the proposed model can be expressed as*

$$\vartheta(\theta) = \vartheta_0 + \frac{\varrho(1-\sigma)\theta^{\varrho-1}g(\theta,\vartheta(\theta))}{M(\sigma)} + \frac{\sigma\varrho}{M(\sigma)}\int_0^\theta y^{\sigma-1}g(y,\vartheta(y))dy, \quad \theta \in \mathbb{I}. \tag{5.5}$$

We introduce the operator $Z : \mathfrak{B} \to \mathfrak{B}$ by

$$Z(\vartheta) = \vartheta_0 + \frac{\varrho(1-\sigma)\theta^{\varrho-1}g(\theta,\vartheta(\theta))}{M(\sigma)} + \frac{\sigma\varrho}{M(\sigma)}\int_0^\theta y^{\sigma-1}g(y,\vartheta(y))dy, \quad \theta \in \mathbb{I}. \tag{5.6}$$

For carrying out the results, we need to take the following necessary assumptions:

(A_1) Let there exist some constants, say $L_g > 0$, such that for $\vartheta, \overline{\vartheta} \in \mathfrak{B}$, we have

$$|g(\theta,\vartheta(\theta)) - g(\theta,\overline{\vartheta}(\theta))| \leq L_g|\vartheta - \overline{\vartheta}|;$$

(A_2) Assume that there exist constants C_g and $M_g > 0$ such that

$$|g(\theta,\vartheta(\theta))| \leq C_g|\vartheta(\theta)| + M_g.$$

Theorem 5.2. *Under assumptions* (A_1) *and* (A_2)*, problem* (5.2) *has at least one solution.*

Proof. For the proof, see [31]. □

Theorem 5.3. *Under assumption* (A_1) *and the condition* $\frac{L_g}{M(\sigma)}\left(\varrho\,(1-\sigma)\,T^{\varrho-1} + \sigma T^{\varrho}\right) < 1$*, the problem of model* (5.2) *has a unique solution.*

Proof. For the proof, see [31]. □

In the coming section, we derive conditions of H-U stability of the proposed model.

6. Hyers-Ulam (H-U) stability

Here, we develop conditions for H-U stability of the proposed SEVAIR model.

Definition 6.1. The model prescribed by (5.2) is H-U stable if there is a real number $\mathbf{c} > 0 \ni$ for each $\epsilon > 0$, any solution $\widehat{\vartheta} \in \mathfrak{B}$ of inequality

$$\left|{}^{PFFCF}D_\theta^{\sigma,\varrho}\widehat{\vartheta}(\theta) - g(\theta,\widehat{\vartheta}(\theta))\right| \leq \epsilon, \theta \in \mathbb{I},$$

and a unique solution $\vartheta \in \mathfrak{B}$ of model (5.2), the following inequality satisfies

$$\left\|\widehat{\vartheta} - \vartheta\right\| \leq \mathbf{c}\epsilon, \qquad \theta \in \mathbb{I},$$

where

$$\widehat{\vartheta}(\theta) = \begin{pmatrix} \widehat{S}(\theta) \\ \widehat{E}(\theta) \\ \widehat{V}(\theta) \\ \widehat{A}(\theta) \\ \widehat{I}(\theta) \\ \widehat{R}(\theta) \end{pmatrix}, \widehat{\vartheta}(0) = \begin{pmatrix} \widehat{S}(0) \\ \widehat{E}(0) \\ \widehat{V}(0) \\ \widehat{A}(0) \\ \widehat{I}(0) \\ \widehat{R}(0) \end{pmatrix}, g(\theta,\widehat{\vartheta}(\theta)) = \begin{pmatrix} \widehat{\vartheta}_1(\theta,\widehat{S},\widehat{E},\widehat{V},\widehat{A},\widehat{I},\widehat{R}) \\ \widehat{\vartheta}_2(\theta,\widehat{S},\widehat{E},\widehat{V},\widehat{A},\widehat{I},\widehat{R}) \\ \widehat{\vartheta}_3(\theta,\widehat{S},\widehat{E},\widehat{V},\widehat{A},\widehat{I},\widehat{R}) \\ \widehat{\vartheta}_4(\theta,\widehat{S},\widehat{E},\widehat{V},\widehat{A},\widehat{I},\widehat{R}) \\ \widehat{\vartheta}_5(\theta,\widehat{S},\widehat{E},\widehat{V},\widehat{A},\widehat{I},\widehat{R}) \\ \widehat{\vartheta}_6(\theta,\widehat{S},\widehat{E},\widehat{V},\widehat{A},\widehat{I},\widehat{R}) \end{pmatrix}.$$

Remark 1. Let there exist a small perturbation $\Psi \in \mathfrak{B}$ such that
(i) $|\Psi(\theta)| \leq \epsilon,\ \theta \in \mathbb{I}$;
(ii) ${}^{PFFCF}D_{\theta}^{\sigma,\varrho}\widehat{\vartheta}(\theta) = g(\theta, \widehat{\vartheta}(\theta)) + \Psi(\theta),\ \theta \in \mathbb{I}$.

A perturbed problem solution is derived by Remark 1,

$$\begin{cases} {}^{PFFCF}D_{\theta}^{\sigma,\varrho}\widehat{\vartheta}(\theta) = g(\theta, \widehat{\vartheta}(\theta)) + \Psi(\theta), \\ \widehat{\vartheta}(0) = \widehat{\vartheta}_0 > 0. \end{cases} \tag{6.1}$$

Lemma 6.2. *The solution of problem* (6.1) *that has a perturbation function* $\Psi(\theta)$ *is provided by*

$$\widehat{\vartheta}(\theta) = \widehat{\vartheta}_0 + \frac{\varrho(1-\sigma)\theta^{\varrho-1}(g(\theta, \widehat{\vartheta}(\theta)) + \Psi(\theta))}{M(\sigma)} + \frac{\sigma\varrho}{M(\sigma)}\int_0^{\theta} y^{\sigma-1}(g(y, \widehat{\vartheta}(y)) + \Psi(y))dy, \quad \theta \in \mathbb{I}. \tag{6.2}$$

Proof. The proof can be obtained by using Lemma 5.1. □

Theorem 6.3. *Under assumption* (A_1) *and the condition* $\frac{L_g}{M(\sigma)}\left(\varrho\,(1-\sigma)\,T^{\varrho-1} + \sigma T^{\varrho}\right) < 1$, *model* (5.2) *is H-U stable.*

Proof. Let $\vartheta, \widehat{\vartheta} \in \mathfrak{B}$ be unique and any solution of model (5.2) and (6.1), respectively. For $\theta \in (\theta_1, T]$, using (5.5) and (6.2), we have

$$\begin{aligned} &\left|\widehat{\vartheta}(\theta) - \vartheta(\theta)\right| \leq \frac{\varrho(1-\sigma)\theta^{\varrho-1}}{M(\sigma)}\left|g(\theta, \widehat{\vartheta}(\theta)) - g(\theta, \vartheta(\theta))\right| + \frac{\sigma\varrho}{M(\sigma)}\int_0^{\theta} y^{\sigma-1}\left|g(\theta, \widehat{\vartheta}(\theta)) - g(\theta, \vartheta(\theta))\right| dy \\ &+ \frac{\varrho(1-\sigma)\theta^{\varrho-1}}{M(\sigma)}|\Psi(\theta)| + \frac{\sigma\varrho}{M(\sigma)}\int_0^{\theta} y^{\sigma-1}|\Psi(\theta)|\,dy \\ &\leq \frac{L_g}{M(\sigma)}\left(\varrho\,(1-\sigma)\,T^{\varrho-1} + \sigma T^{\varrho}\right)\left\|\widehat{\vartheta} - \vartheta\right\| + \left(\frac{\varrho(1-\sigma)T^{\varrho-1}}{M(\sigma)} + \frac{\varrho}{M(\sigma)}T^{\sigma}\right)\epsilon. \end{aligned} \tag{6.3}$$

Further simplification implies

$$\left\|\widehat{\vartheta} - \vartheta\right\| \leq \frac{\left(\frac{\varrho(1-\sigma)T^{\varrho-1}}{M(\sigma)} + \frac{\varrho}{M(\sigma)}T^{\sigma}\right)}{1 - \left(\frac{L_g}{M(\sigma)}\left(\varrho\,(1-\sigma)\,T^{\varrho-1} + \sigma T^{\varrho}\right)\right)}\epsilon. \tag{6.4}$$

This implies that

$$\left\|\widehat{\vartheta} - \vartheta\right\| \leq \mathbf{c}\epsilon,$$

where

$$\mathbf{c} = \frac{\left(\frac{\varrho(1-\sigma)T^{\varrho-1}}{M(\sigma)} + \frac{\varrho}{M(\sigma)}T^{\sigma}\right)}{1 - \left(\frac{L_g}{M(\sigma)}\left(\varrho\,(1-\sigma)\,T^{\varrho-1} + \sigma T^{\varrho}\right)\right)}. \tag{6.5}$$

This proves that model (5.2) is H-U stable. □

7. Numerical solution of (2.1)

In this section, we aim to find the numerical solution for model (5.2) under FFCFDs. For the numerical simulations, we employed an extended Adams-Bashforth numerical scheme, which is widely used for fractional-order systems. This approach is known to provide reliable approximations with a second-order convergence rate in the fractal-fractional Caputo-Fabrizio setting. While effective, it is not the only available numerical scheme. Recent developments, such as the control parametrization technique reported in [33], achieve second-order convergence and can offer improved computational efficiency. Although a detailed implementation of that method is beyond the scope of this work, we acknowledge its advantages and consider it a promising direction for future research. In this study, we focus on the Adams-Bashforth scheme due to its robustness, simplicity, and ability to capture the qualitative dynamics of the SEVAIR model under fractal-fractional operators. This approach has already been applied to epidemiological models, see [31, 34].

We proceed with the corresponding integral form of the model, at $\theta = \theta_{a+1}$, presented in the following:

$$\begin{cases} S^{a+1} = S(0) + \dfrac{\varrho(1-\sigma)\theta_a^{\varrho-1}\vartheta_1(\theta_a, S, E, V, A, I, R)}{M(\sigma)} + \dfrac{\sigma\varrho}{M(\sigma)}\displaystyle\int_0^{\theta_a} y^{\sigma-1}\vartheta_1(y, S, E, V, A, I, R)dy, \quad \theta_a \in \mathbb{I}, \\ E^{a+1} = E(0) + \dfrac{\varrho(1-\sigma)\theta_a^{\varrho-1}\vartheta_2(\theta_a, S, E, V, A, I, R)}{M(\sigma)} + \dfrac{\sigma\varrho}{M(\sigma)}\displaystyle\int_0^{\theta_a} y^{\sigma-1}\vartheta_2(y, S, E, V, A, I, R)dy, \quad \theta_a \in \mathbb{I}, \\ V^{a+1} = V(0) + \dfrac{\varrho(1-\sigma)\theta_a^{\varrho-1}\vartheta_3(\theta_a, S, E, V, A, I, R)}{M(\sigma)} + \dfrac{\sigma\varrho}{M(\sigma)}\displaystyle\int_0^{\theta_a} y^{\sigma-1}\vartheta_3(y, S, E, V, A, I, R)dy, \quad \theta_a \in \mathbb{I}, \\ A^{a+1} = A(0) + \dfrac{\varrho(1-\sigma)\theta_a^{\varrho-1}\vartheta_4(\theta_a, S, E, V, A, I, R)}{M(\sigma)} + \dfrac{\sigma\varrho}{M(\sigma)}\displaystyle\int_0^{\theta_a} y^{\sigma-1}\vartheta_4(y, S, E, V, A, I, R)dy, \quad \theta_a \in \mathbb{I}, \\ I^{a+1} = I(0) + \dfrac{\varrho(1-\sigma)\theta_a^{\varrho-1}\vartheta_5(\theta_a, S, E, V, A, I, R)}{M(\sigma)} + \dfrac{\sigma\varrho}{M(\sigma)}\displaystyle\int_0^{\theta_a} y^{\sigma-1}\vartheta_5(y, S, E, V, A, I, R)dy, \quad \theta_a \in \mathbb{I}, \\ R^{a+1} = R(0) + \dfrac{\varrho(1-\sigma)\theta_a^{\varrho-1}\vartheta_6(\theta_a, S, E, V, A, I, R)}{M(\sigma)} + \dfrac{\sigma\varrho}{M(\sigma)}\displaystyle\int_0^{\theta_a} y^{\sigma-1}\vartheta_6(y, S, E, V, A, I, R)dy, \quad \theta_a \in \mathbb{I}. \end{cases} \tag{7.1}$$

We then approximate the systems as

$$\begin{cases} S^{a+1} = \begin{cases} S(0) + \frac{\varrho(1-\sigma)\theta_a^{\varrho-1}\vartheta_1(\theta_a,S^a,E^a,V^a,A^a,I^a,R^a)}{M(\sigma)} - \frac{\varrho(1-\sigma)\theta_{a-1}^{\varrho-1}\vartheta_1(\theta_{a-1},S^{a-1},E^{a-1},V^{a-1},A^{a-1},I^{a-1},R^{a-1})}{M(\sigma)} \\ \quad + \frac{\sigma\varrho}{M(\sigma)}\int_{\theta_a}^{\theta_{a+1}} y^{\sigma-1}\vartheta_1(y,S,E,V,A,I,R)dy, \quad \theta_a,\theta_{a+1}\in\mathbb{I}, \end{cases} \\ E^{a+1} = \begin{cases} E(0) + \frac{\varrho(1-\sigma)\theta_a^{\varrho-1}\vartheta_2(\theta_a,S^a,E^a,V^a,A^a,I^a,R^a)}{M(\sigma)} - \frac{\varrho(1-\sigma)\theta_{a-1}^{\varrho-1}\vartheta_2(\theta_{a-1},S^{a-1},E^{a-1},V^{a-1},A^{a-1},I^{a-1},R^{a-1})}{M(\sigma)} \\ \quad + \frac{\sigma\varrho}{M(\sigma)}\int_{\theta_a}^{\theta_{a+1}} y^{\sigma-1}\vartheta_2(y,S,E,V,A,I,R)dy, \quad \theta_a,\theta_{a+1}\in\mathbb{I}, \end{cases} \\ V^{a+1} = \begin{cases} V(0) + \frac{\varrho(1-\sigma)\theta_a^{\varrho-1}\vartheta_3(\theta_a,S^a,E^a,V^a,A^a,I^a,R^a)}{M(\sigma)} - \frac{\varrho(1-\sigma)\theta_{a-1}^{\varrho-1}\vartheta_3(\theta_{a-1},S^{a-1},E^{a-1},V^{a-1},A^{a-1},I^{a-1},R^{a-1})}{M(\sigma)} \\ \quad + \frac{\sigma\varrho}{M(\sigma)}\int_{\theta_a}^{\theta_{a+1}} y^{\sigma-1}\vartheta_3(y,S,E,V,A,I,R)dy, \quad \theta_a,\theta_{a+1}\in\mathbb{I}, \end{cases} \\ A^{a+1} = \begin{cases} A(0) + \frac{\varrho(1-\sigma)\theta_a^{\varrho-1}\vartheta_4(\theta_a,S^a,E^a,V^a,A^a,I^a,R^a)}{M(\sigma)} - \frac{\varrho(1-\sigma)\theta_{a-1}^{\varrho-1}\vartheta_4(\theta_{a-1},S^{a-1},E^{a-1},V^{a-1},A^{a-1},I^{a-1},R^{a-1})}{M(\sigma)} \\ \quad + \frac{\sigma\varrho}{M(\sigma)}\int_{\theta_a}^{\theta_{a+1}} y^{\sigma-1}\vartheta_4(y,S,E,V,A,I,R)dy, \quad \theta_a,\theta_{a+1}\in\mathbb{I}, \end{cases} \\ I^{a+1} = \begin{cases} I(0) + \frac{\varrho(1-\sigma)\theta_a^{\varrho-1}\vartheta_5(\theta_a,S^a,E^a,V^a,A^a,I^a,R^a)}{M(\sigma)} - \frac{\varrho(1-\sigma)\theta_{a-1}^{\varrho-1}\vartheta_5(\theta_{a-1},S^{a-1},E^{a-1},V^{a-1},A^{a-1},I^{a-1},R^{a-1})}{M(\sigma)} \\ \quad + \frac{\sigma\varrho}{M(\sigma)}\int_{\theta_a}^{\theta_{a+1}} y^{\sigma-1}\vartheta_5(y,S,E,V,A,I,R)dy, \quad \theta_a,\theta_{a+1}\in\mathbb{I}, \end{cases} \\ R^{a+1} = \begin{cases} R(0) + \frac{\varrho(1-\sigma)\theta_a^{\varrho-1}\vartheta_6(\theta_a,S^a,E^a,V^a,A^a,I^a,R^a)}{M(\sigma)} - \frac{\varrho(1-\sigma)\theta_{a-1}^{\varrho-1}\vartheta_6(\theta_{a-1},S^{a-1},E^{a-1},V^{a-1},A^{a-1},I^{a-1},R^{a-1})}{M(\sigma)} \\ \quad + \frac{\sigma\varrho}{M(\sigma)}\int_{\theta_a}^{\theta_{a+1}} y^{\sigma-1}\vartheta_6(y,S,E,V,A,I,R)dy, \quad \theta_a,\theta_{a+1}\in\mathbb{I}. \end{cases} \end{cases} \tag{7.2}$$

Employing Lagrangian polynomials for piecewise interpolation, and integrating, we find

$$S^{a+1} = \begin{cases} S(0) + \frac{\varrho(1-\sigma)\theta_a^{\varrho-1}\vartheta_1(\theta_a,S^a,E^a,V^a,A^a,I^a,R^a)}{M(\sigma)} - \frac{\varrho(1-\sigma)\theta_{a-1}^{\varrho-1}\vartheta_1(\theta_{a-1},S^{a-1},E^{a-1},V^{a-1},A^{a-1},I^{a-1},R^{a-1})}{M(\sigma)} \\ + \frac{\varrho\sigma}{M(\sigma)}\frac{3}{2}(\Delta\theta)\theta_a^{\varrho-1}\vartheta_1(\theta_a,S^a,E^a,V^a,A^a,I^a,R^a) - \frac{\varrho\sigma}{M(\sigma)}\frac{(\Delta\theta)}{2}\theta_{a-1}^{\varrho-1}\vartheta_1(\theta_{a-1},S^{a-1},E^{a-1},V^{a-1},A^{a-1},I^{a-1},R^{a-1}), \\ \theta_a,\theta_{a-1}\in\mathbb{I}, \end{cases}$$

$$E^{a+1} = \begin{cases} E(0) + \frac{\varrho(1-\sigma)\theta_a^{\varrho-1}\vartheta_2(\theta_a,S^a,E^a,V^a,A^a,I^a,R^a)}{M(\sigma)} - \frac{\varrho(1-\sigma)\theta_{a-1}^{\varrho-1}\vartheta_2(\theta_{a-1},S^{a-1},E^{a-1},V^{a-1},A^{a-1},I^{a-1},R^{a-1})}{M(\sigma)} \\ + \frac{\varrho\sigma}{M(\sigma)}\frac{3}{2}(\Delta\theta)\theta_a^{\varrho-1}\vartheta_2(\theta_a,S^a,E^a,V^a,A^a,I^a,R^a) - \frac{\varrho\sigma}{M(\sigma)}\frac{(\Delta\theta)}{2}\theta_{a-1}^{\varrho-1}\vartheta_2(\theta_{a-1},S^{a-1},E^{a-1},V^{a-1},A^{a-1},I^{a-1},R^{a-1}), \\ \theta_a,\theta_{a-1}\in\mathbb{I}, \end{cases}$$

$$V^{a+1} = \begin{cases} V(0) + \frac{\varrho(1-\sigma)\theta_a^{\varrho-1}\vartheta_3(\theta_a,S^a,E^a,V^a,A^a,I^a,R^a)}{M(\sigma)} - \frac{\varrho(1-\sigma)\theta_{a-1}^{\varrho-1}\vartheta_3(\theta_{a-1},S^{a-1},E^{a-1},V^{a-1},A^{a-1},I^{a-1},R^{a-1})}{M(\sigma)} \\ + \frac{\varrho\sigma}{M(\sigma)}\frac{3}{2}(\Delta\theta)\theta_a^{\varrho-1}\vartheta_3(\theta_a,S^a,E^a,V^a,A^a,I^a,R^a) - \frac{\varrho\sigma}{M(\sigma)}\frac{(\Delta\theta)}{2}\theta_{a-1}^{\varrho-1}\vartheta_3(\theta_{a-1},S^{a-1},E^{a-1},V^{a-1},A^{a-1},I^{a-1},R^{a-1}), \\ \theta_a,\theta_{a-1}\in\mathbb{I}, \end{cases}$$

$$
A^{a+1} = \begin{cases} A(0) + \frac{\varrho(1-\sigma)\theta_a^{\varrho-1}\vartheta_4(\theta_a,S^a,E^a,V^a,A^a,I^a,R^a)}{M(\sigma)} - \frac{\varrho(1-\sigma)\theta_{a-1}^{\varrho-1}\vartheta_4(\theta_{a-1},S^{a-1},E^{a-1},V^{a-1},A^{a-1},I^{a-1},R^{a-1})}{M(\sigma)} \\ + \frac{\varrho\sigma}{M(\sigma)}\frac{3}{2}(\Delta\theta)\theta_a^{\varrho-1}\vartheta_4(\theta_a,S^a,E^a,V^a,A^a,I^a,R^a) - \frac{\varrho\sigma}{M(\sigma)}\frac{(\Delta\theta)}{2}\theta_{a-1}^{\varrho-1}\vartheta_4(\theta_{a-1},S^{a-1},E^{a-1},V^{a-1},A^{a-1},I^{a-1},R^{a-1}), \\ \theta_a,\theta_{a-1}\in\mathbb{I}, \end{cases}
$$

$$
I^{a+1} = \begin{cases} I(0) + \frac{\varrho(1-\sigma)\theta_a^{\varrho-1}\vartheta_5(\theta_a,S^a,E^a,V^a,A^a,I^a,R^a)}{M(\sigma)} - \frac{\varrho(1-\sigma)\theta_{a-1}^{\varrho-1}\vartheta_5(\theta_{a-1},S^{a-1},E^{a-1},V^{a-1},A^{a-1},I^{a-1},R^{a-1})}{M(\sigma)} \\ + \frac{\varrho\sigma}{M(\sigma)}\frac{3}{2}(\Delta\theta)\theta_a^{\varrho-1}\vartheta_5(\theta_a,S^a,E^a,V^a,A^a,I^a,R^a) - \frac{\varrho\sigma}{M(\sigma)}\frac{(\Delta\theta)}{2}\theta_{a-1}^{\varrho-1}\vartheta_5(\theta_{a-1},S^{a-1},E^{a-1},V^{a-1},A^{a-1},I^{a-1},R^{a-1}), \\ \theta_a,\theta_{a-1}\in\mathbb{I}, \end{cases}
$$

$$
R^{a+1} = \begin{cases} R(0) + \frac{\varrho(1-\sigma)\theta_a^{\varrho-1}\vartheta_6(\theta_a,S^a,E^a,V^a,A^a,I^a,R^a)}{M(\sigma)} - \frac{\varrho(1-\sigma)\theta_{a-1}^{\varrho-1}\vartheta_6(\theta_{a-1},S^{a-1},E^{a-1},V^{a-1},A^{a-1},I^{a-1},R^{a-1})}{M(\sigma)} \\ + \frac{\varrho\sigma}{M(\sigma)}\frac{3}{2}(\Delta\theta)\theta_a^{\varrho-1}\vartheta_6(\theta_a,S^a,E^a,V^a,A^a,I^a,R^a) - \frac{\varrho\sigma}{M(\sigma)}\frac{(\Delta\theta)}{2}\theta_{a-1}^{\varrho-1}\vartheta_6(\theta_{a-1},S^{a-1},E^{a-1},V^{a-1},A^{a-1},I^{a-1},R^{a-1}), \\ \theta_a,\theta_{a-1}\in\mathbb{I}. \end{cases} \tag{7.3}
$$

In the next section, the solution given in Eq (7.3) is employed to perform the numerical simulations.

8. Numerical simulations and analysis

In this section, we present numerical simulations that illustrate the time evolution of the SEVAIR system. The parameter values adopted for our simulations are summarized in Table 1. They represent key biological processes in adenovirus transmission: ζ and ζ_a describe the transmission rates from symptomatic and asymptomatic individuals, respectively, η reflects the short incubation period of adenovirus conjunctivitis, k is the proportion of vaccinated-exposed individuals who become asymptomatic, γ is the vaccinated-to-infected progression rate, b and q represent recovery and quarantine rates for symptomatic cases, respectively, while ρ and β account for natural birth and death rates in the population, respectively.

These values are illustrative rather than fitted to real outbreak data and are chosen to highlight the dynamics for acute hemorrhagic conjunctivitis, consistent with the parameter values used in [29].

The trajectories of the susceptible, exposed, asymptomatic, symptomatic, vaccinated, and recovered populations are plotted to highlight their dynamics. These results provide an intuitive picture of how the disease spreads through different transmission routes. To further enhance clarity, we include a comparison chart that contrasts the contributions of asymptomatic and symptomatic pathways, thereby supporting the theoretical deductions with visual evidence.

We simulate the numerical results under fractional-order and fractal-dimensional variations to observe the dynamics of the different compartments in the proposed SEVAIR model. All numerical simulations were executed using MATLAB R2023a, providing a robust and reliable environment for implementing the algorithms and analyzing the system's dynamic behavior.

As a first simulation, we plot the dynamical behavior of all compartments in a single figure, as shown in Figure 2.

In Figures 3–8, the fractal dimension is fixed at 0.65 while the fractional order is varied to examine its effect on the model dynamics. The figures display the evolution of all compartments (Susceptible, Exposed, Vaccinated, Asymptomatic, Infected, and Recovered) under different fractional orders. As the fractional order increases, the solutions become smoother and stabilize more rapidly. In contrast, lower orders reflect stronger memory effects, often causing delayed convergence or oscillations. This demonstrates the model's sensitivity to memory effects governed by the fractional parameter σ.

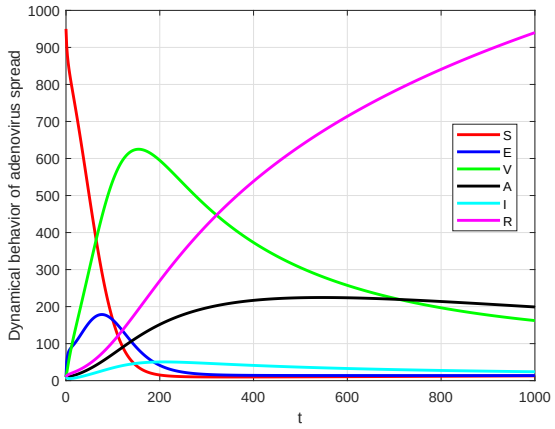

Figure 2. Dynamical behavior of the SEVAIR model taking $\sigma = 0.95$ and $\varrho = 0.65$.

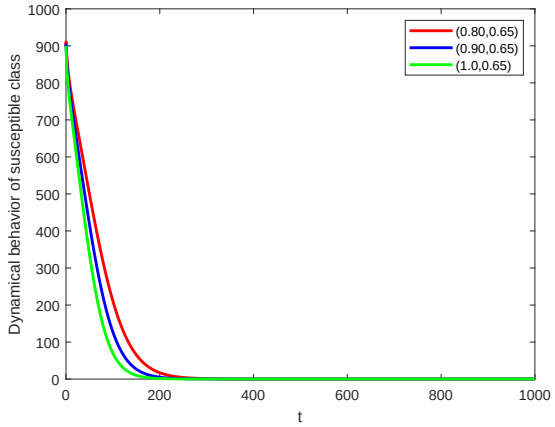

Figure 3. Dynamical behavior of the susceptible class on various fractional orders with the same fractal dimension.

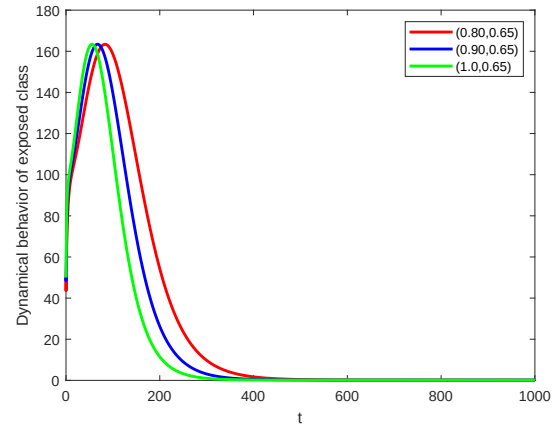

Figure 4. Dynamical behavior of the exposed class on various fractional orders with the same fractal dimension.

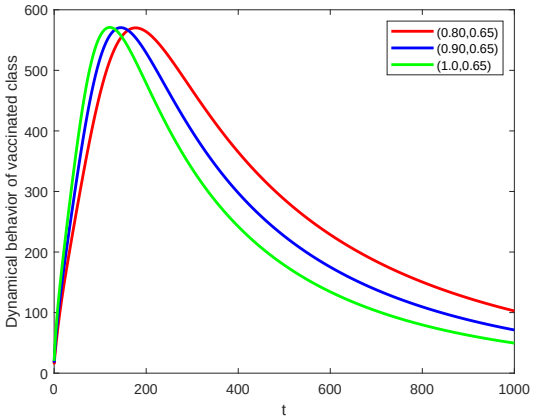

Figure 5. Dynamical behavior of the vaccinated class on various fractional orders with the same fractal dimension.

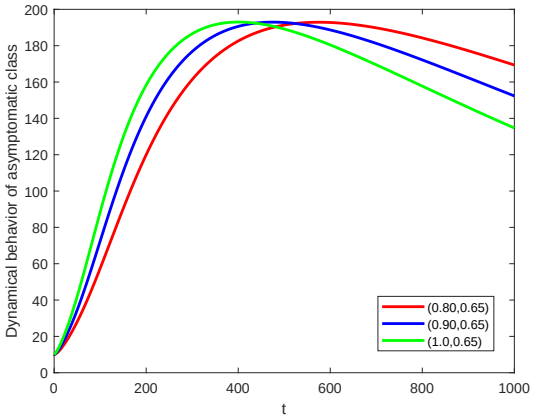

Figure 6. Dynamical behavior of the recovered class on various fractional orders with the same fractal dimension.

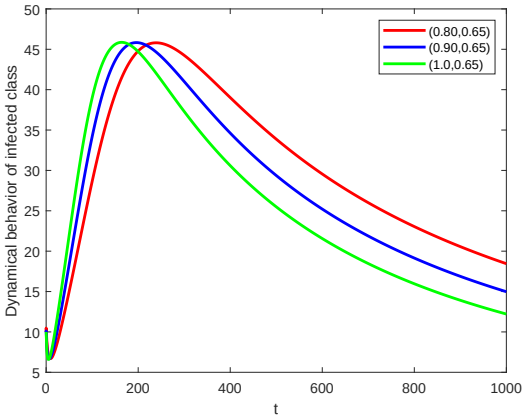

Figure 7. Dynamical behavior of the infected class on various fractional orders with the same fractal dimension.

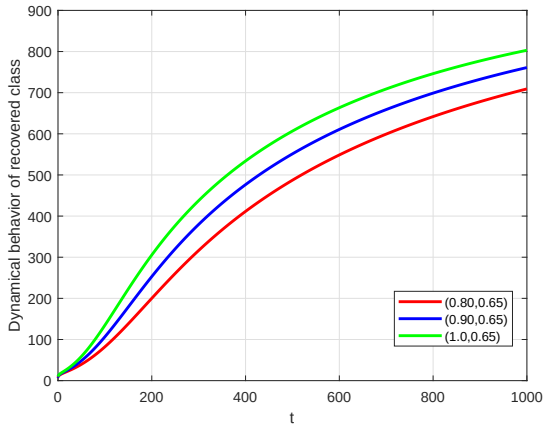

Figure 8. Dynamical behavior of the recovered class on various fractional orders with the same fractal dimension.

In Figures 9–14, the fractional order is kept constant while the fractal dimension is varied to examine its impact on the model's dynamics. These figures show how changes in fractal dimension values influence each compartment, with the fractional order fixed. The fractal dimension reflects structural irregularities and heterogeneity in population behavior. As it increases, the dynamics generally exhibit greater complexity and faster peak responses—particularly in the exposed, vaccinated, asymptomatic, and infected compartments. This suggests that more intricate population structures may drive more intense epidemic waves.

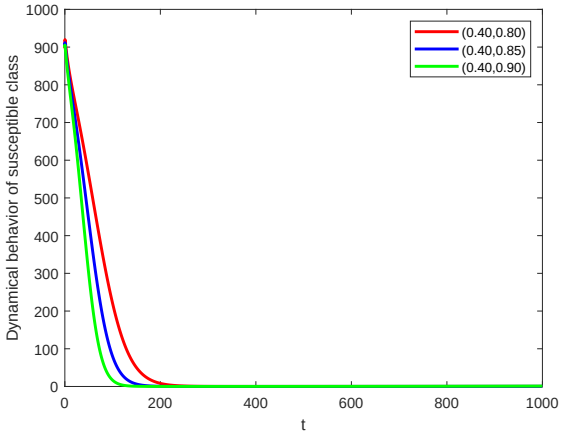

Figure 9. Dynamical behavior of the susceptible class on various fractal dimensions with fixed fractional orders.

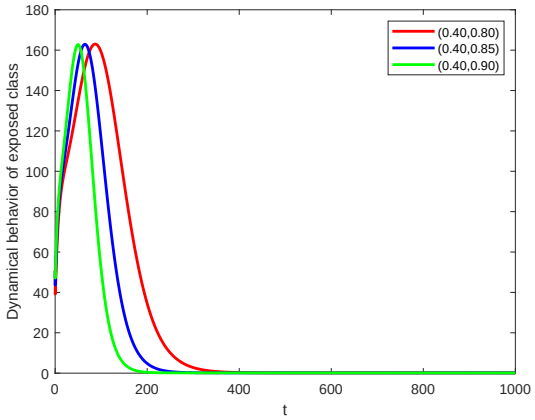

Figure 10. Dynamical behavior of the exposed class on various fractal dimensions with fixed fractional orders.

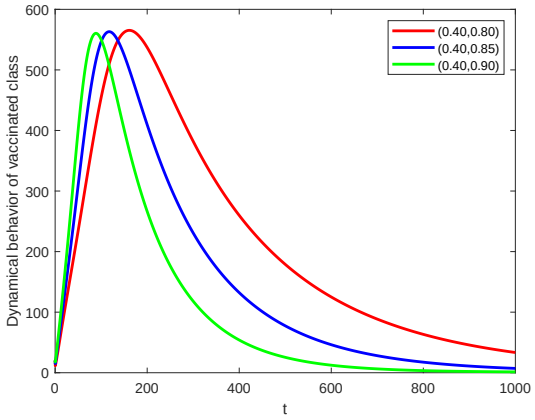

Figure 11. Dynamical behavior of the vaccinated class on various fractal dimensions with fixed fractional orders.

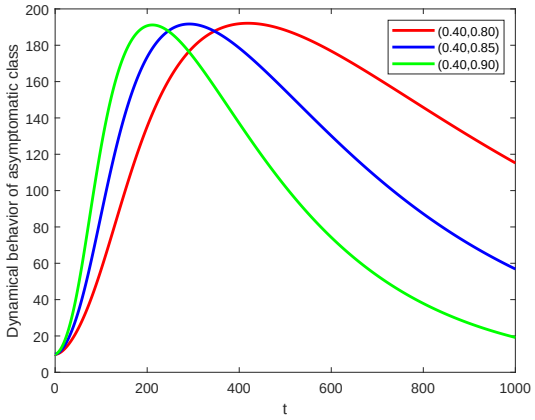

Figure 12. Dynamical behavior of the vaccinated class on various fractal dimensions with fixed fractional orders.

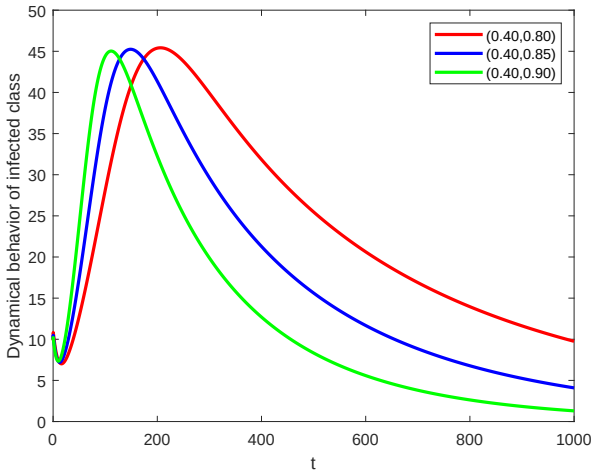

Figure 13. Dynamical behavior of the infected class on various fractal dimensions with fixed fractional orders.

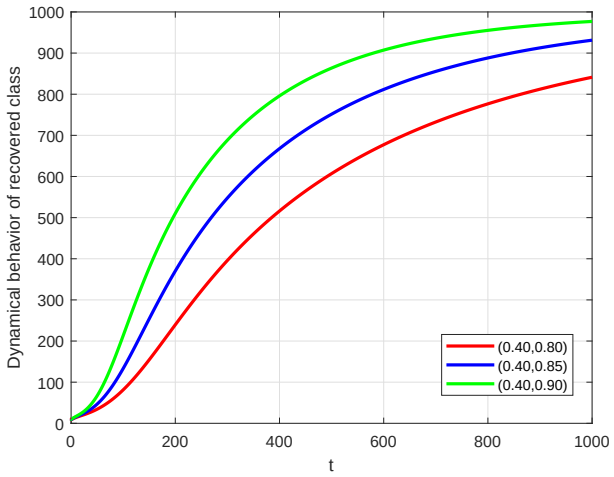

Figure 14. Dynamical behavior of the recovered class on various fractal dimensions with fixed fractional orders.

Across all figures, the interaction between fractional order and fractal dimension offers nuanced control over the system's behavior. Such sensitivity analysis is essential for fitting real-world data and capturing diverse epidemic patterns. Notably, the asymptomatic class is especially responsive to both parameters, underscoring its critical role in modeling adenovirus transmission.

In the Figure 15, the stacked-area plot compares the instantaneous contributions of symptomatic and asymptomatic transmission to new exposures. This clarifies the role of asymptomatic carriers in driving the epidemic under the fractal-fractional operator.

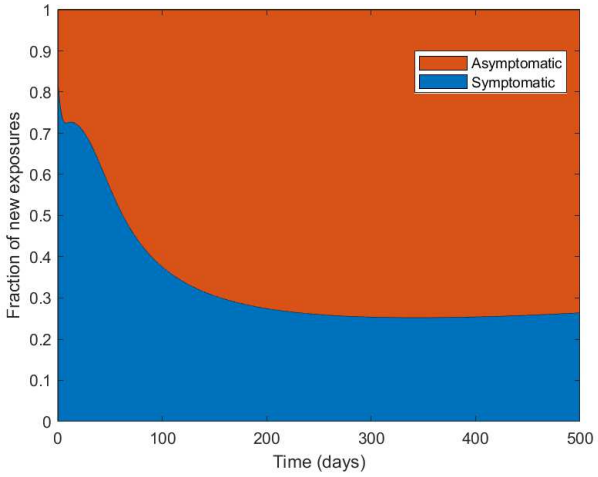

Figure 15. Contributions to new exposures using $\sigma = 0.95$ and $\varrho = 1$.

9. Conclusions

This research introduced an enhanced SEVAIR model to better represent the spread of adenovirus by accounting for individuals who carry the virus without showing symptoms. By integrating the fractal-fractional Caputo-Fabrizio operator with a power-law kernel, the model effectively captures memory and hereditary traits in the disease's transmission. Through rigorous mathematical techniques, including fixed point theory and H-U stability, we established the existence and stability of solutions. The model's critical thresholds, such as the basic reproduction number, were derived to assess the potential for outbreaks. Numerical simulations using a refined Adams-Bashforth method confirmed the analytical outcomes and revealed the significant influence of the asymptomatic population on disease dynamics.

The present study is based on certain simplifying assumptions that should be acknowledged. In particular, the model does not explicitly incorporate age structure, spatial heterogeneity, or possible virus mutations, all of which can influence transmission dynamics in real-world settings. These simplifications were made to keep the analysis tractable, but they also indicate potential directions for future work. Incorporating demographic structure, mobility patterns, and viral variability into fractional-order epidemic models may provide a more comprehensive understanding of adenovirus transmission and intervention strategies. Despite these limitations, the current framework provides important insights into the roles of vaccination and asymptomatic carriers in shaping epidemic outcomes and offers a basis for further refinement in more realistic contexts.

In this study, parameters were selected solely to examine the qualitative dynamics of the system under varying fractal-fractional orders, without data fitting. A valuable future direction is the systematic estimation and validation of parameters for the fractional-order model, as memory effects influence coefficient scaling. Advanced estimation methods, such as those in [32], could ensure dimensional consistency and improve alignment with epidemiological data. Such calibration would enhance forecasting accuracy, support intervention assessments, and increase the model's practical relevance for public health decision-making.

Author contributions

M. S. Algolam and A. Ali: Conceptualization; A. Ali, K. Aldwoah and A. Alsulami: Methodology; K. Aldwoah, M. Rabih and M. M. Abdelwahab: Formal analysis; M. S. Algolam, A. Alsulami and M. M. Abdelwahab: Investigation; M. Rabih: Software; M. Rabih and M. M. Abdelwahab: Visualization; A. Ali: Writing – original draft; K. Aldwoah and A. A. Qurtam: Supervision; A. A. Qurtam: Funding acquisition; A. A. Qurtam, A. Alsulami and M. M. Abdelwahab: Writing – review & editing. All the authors have read and agreed to the published version of the manuscript.

Use of Generative-AI tools declaration

The authors declare that no artificial intelligence (AI) tools were used in the writing, analysis, or preparation of this article.

Funding

This work was supported and funded by the Deanship of Scientific Research at Imam Mohammad Ibn Saud Islamic University (IMSIU) (grant number IMSIU-DDRSP2501).

Conflict of interest

The authors declare no competing financial or personal interests influencing this work.

References

1. *Center for Disease Control (CDC)*, Conjunctivitis (pink eye). Available from: `https://www.cdc.gov`.
2. S. R. Fehily, G. B. Cross, A. J. Fuller, Bilateral conjunctivitis in a returned traveler, *PLoS Neglect. Trop. D.*, **9** (2015), e0003351. https://doi.org/10.1371/journal.pntd.0003351
3. R. H. Elliot, Conjunctivitis in the tropics, *Brit. Med. J.*, **1** (1925), 12–14. https://doi.org/10.1136/bmj.1.3340.12-a
4. K. N. Malu, Allergic conjunctivitis in Jos-Nigeria, *Niger. Med. J.*, **55** (2014), 166–170. https://doi.org/10.4103/0300-1652.129664
5. D. W. Kimberlin, *Red book: 2018-2021 report of the committee on infectious diseases*, 31 Eds., American Academy of Pediatrics: Itasca, IL, USA, 2018.
6. S. Sangsawang, T. Tanutpanit, W. Mumtong, P. Pongsumpun, Local stability analysis of mathematical model for hemorrhagic conjunctivitis disease, *Current Appl. Sci. Technol.*, **12** (2012), 189–197.
7. O. Ghazali, K. B. Chua, K. P. Ng, P. S. Hooi, M. A. Pallansch, M. S. Oberste, et al., An outbreak of acute haemorrhagic conjunctivitis in Melaka, Malaysia, *Singapore Med. J.*, **44** (2003), 511–516.

8. J. Chansaenroj, S. Vongpunsawad, J. Puenpa, A. Theamboonlers, V. Vuthitanachot, P. Chattakul, et al., Epidemic outbreak of acute haemorrhagic conjunctivitis caused by coxsackievirus A24 in Thailand, 2014. *Epidemiol. Infect.*, **143** (2015), 3087–3093. https://doi.org/10.1017/S0950268815000643
9. G. Chowell, E. Shim, F. Brauer, P. Diaz-Dueas, J. M. Hyman, C. Castillo-Chavez, Modelling the transmission dynamics of acute haemorrhagic conjunctivitis: Application to the 2003 outbreak in Mexico, *Stat. Med.*, **25** (2006), 1840–1857. https://doi.org/10.1002/sim.2352
10. J. Suksawat, S. Naowarat, Effect of rainfall on the transmission model of conjunctivitis, *Adv. Environ. Biol.*, **8** (2014), 99–104.
11. B. Unyong, S. Naowarat, Stability analysis of conjunctivitis model with nonlinear incidence term, *Aust. J. Basic Appl. Sci.*, **8** (2014), 52–58.
12. S. Sangthongjeen, A. Sudchumnong, S. Naowarat, Effect of educational campaign on transmission model of conjunctivitis, *Aust. J. Basic Appl. Sci.*, **9** (2015), 811–815.
13. E. K. Yeargers, R. W. Shonkwiler, J. V. Herod, *An introduction to the mathematics of biology: With computer algebra models*, Springer Science & Business Media: New York, NY, USA, 2013, 1–8.
14. K. A. Aldwoah, M. A. Almalahi, M. Hleili, F. A. Alqarni, E. S. Aly, K. Shah, Analytical study of a modified-ABC fractional order breast cancer model, *J. Appl. Math. Comput.*, **70** (2024), 3685–3716. https://doi.org/10.1007/s12190-024-02102-7
15. A. E. Hamza, O. Osman, A. Ali, A. Alsulami, K. Aldwoah, A. Mustafa, et al., Fractal-fractional-order modeling of liver fibrosis disease and its mathematical results with subinterval transitions, *Fractal Fract.*, **8** (2024), 638. https://doi.org/10.3390/fractalfract8110638
16. H. Khan, J. Alzabut, A. Shah, Z. Y. He, S. Etemad, S. Rezapour, et al., On fractal-fractional waterborne disease model: A study on theoretical and numerical aspects of solutions via simulations, *Fractals*, **31** (2023), 2340055. https://doi.org/10.1142/S0218348X23400558
17. T. Alraqad, M. A. Almalahi, N. Mohammed, A. Alahmade, K. A. Aldwoah, Modeling Ebola dynamics with a Φ-piecewise hybrid fractional derivative approach, *Fractal Fract.*, **8** (2024), 596. https://doi.org/10.3390/fractalfract8100596
18. Y. A. Rossikhin, M. V. Shitikova, Application of fractional calculus for dynamic problems of solid mechanics: Novel trends and recent results, *Appl. Mech. Rev.*, **63** (2010), 010801. https://doi.org/10.1115/1.4000563
19. M. S. Algolam, O. Osman, A. Ali, A. Mustafa, K. Aldwoah, A. Alsulami, Fixed point and stability analysis of a tripled system of nonlinear fractional differential equations with n-nonlinear terms, *Fractal Fract.*, **8** (2024), 697. https://doi.org/10.3390/fractalfract8120697
20. M. Naim, Z. Yaagoub, A. Zeb, M. Sadki, K. Allali, Global analysis of a fractional-order viral model with lytic and non-lytic adaptive immunity, *Model. Earth Syst. Environ.*, **10** (2024), 1749–1769. https://doi.org/10.1007/s40808-023-01866-4
21. Z. Yaagoub, M. Sadki, K. Allali, A generalized fractional hepatitis B virus infection model with both cell-to-cell and virus-to-cell transmissions, *Nonlinear Dyn.*, **112** (2024), 16559–16585. https://doi.org/10.1007/s11071-024-09867-3
22. Z. Yaagoub, K. Allali, Fractional HBV infection model with both cell-to-cell and virus-to-cell transmissions and adaptive immunity, *Chaos Soliton. Fract.*, **165** (2022), 112855. https://doi.org/10.1016/j.chaos.2022.112855

23. Z. Yaagoub, Fractional two-strain SVLIR epidemic model with vaccination and quarantine strategies, *Int. J. Dynam. Control*, **13** (2025), 55. https://doi.org/10.1007/s40435-024-01561-x
24. Z. Yaagoub, A. El Bhih, K. Allali, Global analysis of a fractional-order infection model for the propagation of computer viruses, *Model. Earth Syst. Environ.*, **11** (2025), 68. https://doi.org/10.1007/s40808-024-02270-2
25. M. Caputo, M. Fabrizio, A new definition of fractional derivative without singular kernel, *Prog. Fract. Differ. Appl.*, **1** (2015), 73–85.
26. A. Atangana, Fractal-fractional differentiation and integration: Connecting fractal calculus and fractional calculus to predict complex system, *Chaos Soliton. Fract.*, **102** (2017), 396–406. https://doi.org/10.1016/j.chaos.2017.04.027
27. K. Shah, T. Abdeljawad, Study of radioactive decay process of uranium atoms via fractals-fractional analysis, *S. Afr. J. Chem. Eng.*, **48** (2024), 63–70. https://doi.org/10.1016/j.sajce.2024.01.003
28. A. Shah, H. Khan, M. De la Sen, J. Alzabut, S. Etemad, C. T. Deressa, On non-symmetric fractal-fractional modeling for ice smoking: Mathematical analysis of solutions, *Symmetry*, **15** (2022), 87. https://doi.org/10.3390/sym15010087
29. F. Javed, A. Ahmad, A. H. Ali, E. Hincal, A. Amjad, Investigation of conjunctivitis adenovirus spread in human eyes by using bifurcation tool and numerical treatment approach, *Phys. Scr.*, **99** (2024), 085253. https://doi.org/10.1088/1402-4896/ad62a5
30. K. S. Nisar, A. Ahmad, M. Farman, E. Hincal, A. Zehra, Modeling and mathematical analysis of fractional order eye infection (conjunctivitis) virus model with treatment impact: Prelicence and dynamical transmission, *Alex. Eng. J.*, **107** (2024), 33–46. https://doi.org/10.1016/j.aej.2024.07.020
31. R. Sidaoui, W. E. Ahmed, A. Ali, M. Rabih, A. Alsulami, K. Aldwoah, et al., Mathematical and numerical analysis of a SEVIR-S model for adenovirus with immunity waning and reinfection effects, *AIMS Math.*, **10** (2025), 16291–16316. https://doi.org/10.3934/math.2025728
32. C. Liu, X. Yi, Y. Feng, Modelling and parameter identification for a two-stage fractional dynamical system in microbial batch process, *Nonlinear Anal. Model. Control*, **27** (2022), 350–367. https://doi.org/10.15388/namc.2022.27.26234
33. C. Liu, X. Yi, Z. Gong, M. Han, The control parametrization technique for numerically solving fractal-fractional optimal control problems involving Caputo-Fabrizio derivatives, *J. Comput. Appl. Math.*, **472** (2026), 116814. https://doi.org/10.1016/j.cam.2025.116814
34. R. Sidaoui, A. A. Qurtam, A. Ali, M. Suhail, K. Aldwoah, A. Elsayed, et al., Modeling rotavirus transmission with booster vaccination using fractal-fractional derivatives, *AIMS Math.*, **10** (2025), 20025–20049. https://doi.org/10.3934/math.2025895

AIMS Press